Grafting Copper Atoms and Nanoparticles on Double-Walled Carbon Nanotubes: Application to Catalytic Synthesis of Propargylamine

David Mesguich, Lilian Moumaneix, Victor Henri, Morgan Legnani, V. Collière, Jérôme Esvan, Armelle Ouali, Pierre Fau

Grafting Copper Atoms and Nanoparticles on Double-Walled Carbon Nanotubes: Application to Catalytic Synthesis of Propargylamine

David Mesguich,* Lilian Moumaneix, Victor Henri, Morgan Legnani, Vincent Collière, Jérôme Esvan, Armelle Ouali,* and Pierre Fau*

ABSTRACT: The decoration of carbon nanotubes (CNTs) by metal nanoparticles (NPs) combines the advantages of a high specific surface material with catalytic properties of metal nanocrystals. Little work has been devoted to the decoration of CNTs with copper NPs, and no evidence of copper atomic decoration of CNTs has shown up until now. Herein, we demonstrate that the strong acidic oxidation of double walled CNTs (dwCNTs) is very efficient for the decoration of the carbon surface by copper NPs and atoms. This treatment severely degraded the CNT walls and generated a large amount of disordered sp^3 carbon. This amorphous carbon film bears many chemically active functions like carboxyl and hydroxyl ones. In such conditions, the CNT walls behave as very efficient ligands for the stabilization of copper obtained by the thermolysis of the mesityl precursor in organic solution under mild dihydrogen pressure. In addition to copper NPs, we evidenced the presence of a regular coverage with copper atoms over the dwCNTs. This nanocomposite catalyzes the quantitative synthesis of propargylamines via one A^3 type coupling reaction. Five consecutive catalytic cycles with 100% yield could be performed with no loss of activity, and the combination of Cu supported on dwCNTs allows a facile recycling of the catalytic material.

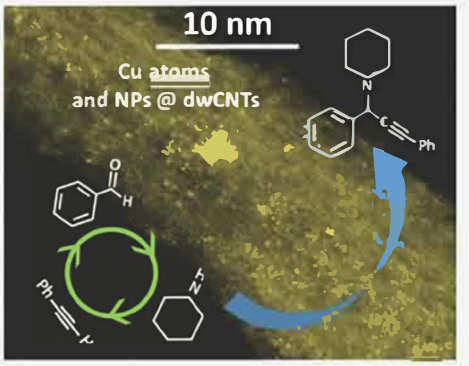

INTRODUCTION

The preparation of nanocomposite materials relying on metal nanoparticles (NPs) grafted on carbon nanotubes (CNTs) nowadays generates an exciting research activity, up to the tremendous expectations it evokes in many technological fields. Many of these applications target important research fields such as catalysis,[1] photocatalysis,[2] H_2 production and storage,[3−5] microelectronics,[6] gas sensors,[7] or biotechnologies.[8,9] Recent improvements in new materials notably concern synthetic methods for combining CNTs and NPs, and they benefit from the increasing power of surface analysis tools (NP/CNT growth and their interactions, molecular bonding of ligands on surfaces, CNT functionalization, ...).[10] There exists a large variety of methods to prepare hybrid NPS@CNTs materials presenting a homogeneous dispersion of metal nanocrystals at the CNT surface. Various physical techniques (evaporation, sputtering of a metal target, ...) as well as chemical ones (electroless or electrochemistry, metallic salts impregnation, ...) have been used to aim at the decoration of CNTs with well controlled NPs in shape and size. Physical processes generally require costly setups (systems running under secondary vacuum level), but in contrast, they offer the great advantage of not using organic surfactants for the stabilization of metallic NPs. However, the NPs' size and size distribution often remain difficult to master. In contrast, chemical routes permit easier access to the control of the deposited NPs. They often involve the use of organic ligands or polymers that play a key role for the nucleation, growth, or stabilization of the NPs.[11−13] Efficient catalytic reactions need a large number of active surface sites on metal NPs. However, organic ligands may hinder these sites and decrease the overall catalytic yield. Therefore, it is highly relevant to develop chemical methods to prepare organic ligand free NPs immobilized onto CNT substrates. In that aim, the CNTs have to be surface functionalized to maximize the number of surface anchoring chemical functions for metal NPs, such as surface carboxyl groups.[14] Most of the literature on the deposition of metal NPs on CNTs deals with noble metals (Au, Ag, Pt, Pd, ...).[15] Due to the reactivity of Cu with oxygen, the decoration of CNTs with Cu NPs remains a challenging process, and few results have been published up to now.[16−18] In the hydrogenolysis of metalorganic precursor implementa

https://doi.org/10.1021/acs.langmuir.2c00771

tion, the synthetic conditions conduce to the formation of metallic copper nanoparticles as shown in the previous work of our team.[19] For example, Silva et al. used Cu acetate in dimethylformamide to decorate single wall CNTs (swCNTs) functionalized by pyrrolidine groups anchored at their surface.[20] The homogeneous decoration with Cu NPs is not obvious, and only a partial reduction of the metal salt has been obtained. Lomeli Rosales et al. presented a single pot methodology to graft Cu NPs on multiwalled CNTs (mwCNTs) by H_2 reduction of Cu mesityl precursors in the presence of N heterocyclic carbene ligands.[21] The mean size of Cu NPs on the mwCNTs is 6 (±1.3) nm which is similar to the measured distribution of Cu NPs in the pure colloidal form, i.e., at the exclusion of the CNTs. This result confirms the major role of the carbene ligands on the stabilization of the Cu NPs in the presence or absence of CNTs. In another implementation,[22] acidified mwCNTs have been decorated with Cu NPs (mean size 7.05 nm) obtained by the reduction of CuCl or $CuSO_4$ salts by $NaBH_4$. Recently, N doped large mwCNTs have been decorated with Cu NPs obtained by impregnation with copper acetate in water.[23] The Cu NPs, which have sizes of 8−10 nm, remain metallic even after an air exposure during 30 days. The composite material was successfully used as a catalyst for one A^3 type coupling reaction where the mixture of aldehyde, a cyclic amine, and an alkyne leads to the formation of propargylamine derivatives. Four consecutive cycles could be successfully achieved, while a decrease of the catalytic activity was observed during the fifth cycle (80% instead of 95−99% of aldehyde conversion). Moreover, the composite underwent a severe mechanical degradation (cracking of the CNT support) evidenced by scanning electron microscopy (SEM). In this paper, we present a protocol to yield stable Cu@CNT nanocomposites that relies first on the functionalization of double walled CNTs (dwCNTs) by successive acidic treatments. The synthesis of Cu NPs is obtained by the soft thermal (110 °C) decomposition of two different metallorganic copper pre cursors in anisole, mesityl copper, and *N,N′* diisopropylaceta midinate copper, in the presence of a moderate dihydrogen pressure (3 bar). No additional molecular ligands are added in the reaction medium as the functionalized CNT surface is expected to play the role of ligands. In this study, nucleation sites formed on acidified CNTs in conjugation with the CuMes precursor allowed the growth of small size Cu NPs (ca. 9 nm) regularly dispersed on the dwCNTs. Remarkably, beyond the homogeneous decoration of CNTs with Cu NPs, we also evidenced the continuous covering of dwCNTs by Cu under the atomic form. This resulted from the presence of a high density of metal coordination sites on the carbonaceous substrates due to the preliminary strong acidic treatment. The catalytic performance of the nanocomposite of this study has been successfully assessed in one A^3 type coupling reaction. The atomic distribution of Cu may be of help for many efficient catalytic reactions.[24]

EXPERIMENTAL SECTION

Materials and Reagents. The *N,N′* diisopropylacetamidinate copper(I) (CuAmd) precursor was synthesized in our laboratory according to a procedure described by Li et al.[25] Copper mesityl (CuMes) was purchased from NanoMePS S.A. and used without further purification. Piperidine (99%), phenylacetylene (98%), and dry anisole ($CH_3OC_6H_5$) were purchased from Sigma Aldrich, and the latter was purified on molecular sieves before use. Tetrahydrofur an (THF) was dried using the MBRAUN purification system. Benzaldehyde was purchased from Alfa Aesar and freshly distilled before use. Hydrochloric acid (37%), nitric acid (65%), and sulfuric acid (95% min) were purchased from VWR Chemicals. All experiments for the preparation of Cu NPs were conducted under pure Ar atmosphere using a glovebox (MBRAUN) and standard Fischer−Porter techniques on vacuum ramps. H_2 gas was provided by Air Liquide Alphagaz 1 grade, purity 99.999%. Catalytic reactions were performed under nitrogen atmosphere using the standard Schlenk technique.

DwCNT Preparation and Functionalization. The dwCNTs were synthesized by chemical catalytic vapor deposition (CCVD) according to the work of Flahaut et al.[26] The CNTs grew from a H_2−CH_4 flow (18% mol. CH_4, 15 L/h) on a Co:Mo MgO based catalyst powder, with the elemental composition $Mg_{0.99}Co_{0.0075}Mo_{0.0025}$, and were placed in a furnace heated up to 1000 °C. This method allowed good structural control and high selectivity since up to 80% of the CNTs were dwCNTs. The obtained composite powder was sonicated for 10 min in an aqueous hydrochloric acid solution before being left overnight at room temperature in order to dissolve all the MgO and all the unprotected Mo and Co nanoparticles. The resulting suspension was washed with deionized water yielding eventually to the pristine CNT suspension. It is noteworthy that despite the sonication treatment, the CNTs often self assembled into bundles due to van der Waals interactions and high specific surface area (980 m^2/g). Pristine CNTs presented two major impurities: Co:Mo carbon encapsulated nanoparticles originating from the metal oxide catalytic powder and residual diaphanous carbon (graphene like disorganized carbon) from which nanotubes often emerged. At this stage, it was still necessary to proceed to additional purification treatments for fully removing Co:Mo nanoparticles and other carbon impurities. Pristine dwCNTs were functionalized by a double acidic treatment: the first HNO_3 stage consisted of refluxing the CNTs (1 g/L) at constant stirring (500 rpm) in a 3 M solution of HNO_3 for 24 h. The second stage of the double oxidation treatment took place immediately after the first HNO_3 treatment. The CNTs were heated under constant stirring (500 rpm) in a 1:3 vol. solution of HNO_3/H_2SO_4 at 70 °C during 5 h in reflux conditions. A detailed investigation of the functionalization of dwCNTs has been previously reported by our team.[27]

Cu Deposition on dwCNTs. An aqueous suspension of dwCNTs (1 g/L) was frozen in liquid nitrogen, freeze dried to avoid agglomeration, and then transferred into a glovebox under N_2. For the decoration with Cu, 10 mg of CNTs was weighted and dispersed in 10 mL of anhydrous anisole. The desired CNT dispersion was obtained with an ultrasonic treatment (150 W, 20 kHz, 5 min).

The CuMes precursor (29 mg, 0.159 mmol) or the CuAmd precursor (32 mg, 0.156 mmol) was introduced under a controlled atmosphere in the Fischer−Porter bottle containing the dwCNTs. The concentration of the metal precursors corresponded to 1 mg of Cu per mL of anisole. The Fischer−Porter reactor was purged with Ar, then placed under vacuum, and finally pressurized by 3 bar of H_2. The vessel was placed in an oil bath at the temperature of 110 °C under a constant magnetic stirring. The reaction was left running 12 h to yield Cu@dwCNTs. At the end of the reaction, the reactor was cooled down to room temperature, and H_2 was replaced by Ar. The Cu@dwCNTs were rinsed with 20 mL of fresh anisole in glovebox conditions and dried at room temperature. The copper amount deposited on the dwCNTs directly depended on the introduced precursor amount (i.e., 6.5 and 3.25 theoretical at % experimentally gave rise to 5.7 and 3.3. at %, respectively).

Characterizations. Transmission electron microscopy (TEM) images of sample were obtained with a JEOL 1400 transmission electron microscope operating at 120 kV. High resolution TEM images were obtained on a JEOL JEM ARM 200f operating at 200 kV. The system had a probe corrector and was equipped with a STEM HAADF detector (scanning TEM high angle annular dark field) for which the contrast of the image depended on the atomic number (Z contrast). It was also equipped with an EDX (energy dispersion X ray) analysis system. X ray photoelectron spectroscopy (XPS) analysis

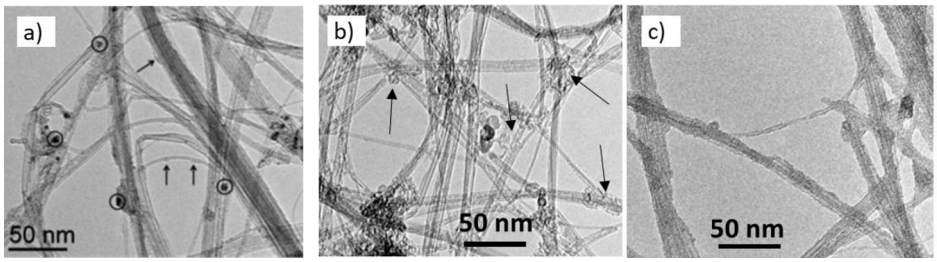

Figure 1. TEM image of CNTs oxidized by acidic solutions: a) pristine CNTs (Arrows indicate the presence diaphanous carbon; circles indicate the presence of a few Co:Mo nanoparticles.), b) single oxidation (Arrows indicate the presence of CCF zones between CNT bundles.), and c) double oxidation (CNTs are arranged in bundles regularly covered by CCFs.).

was performed using a Thermoelectron K alpha device. The photoelectron emission spectra were recorded using Al−Kα radiation ($h\nu$ = 1486.6 eV) from a monochromatized source. The spot size was 400 μm. The pass energy was fixed at 40 eV for a narrow scan and 150 eV for the survey. The spectrometer energy calibration was made using the Au $4f^{7/2}$ (83.9 ± 0.2 eV) and Cu $2p^{3/2}$ (932.8 ± 0.2 eV) photoelectron lines. XPS spectra were recorded in direct N(Ec). The background signal was removed using the Shirley method. The binding energy scale was established by referencing the C 1s value of adventitious carbon (284.6 eV). The photoelectron peaks were analyzed by Lorentzian/Gaussian (L/G = 30) peak fitting. Nuclear magnetic resonance (NMR) spectra were recorded with Bruker 400 MHz equipment at room temperature in the indicated deuterated solvents. ^{1}H NMR spectra were evaluated in parts per million (ppm), and coupling constants (J) were reported in Hertz (Hz). The signals in the spectra were described as s (singlet), d (doublet), t (triplet), and m (multiplet). Gas chromatography mass spectra (GC MS) were recorded on a Shimadzu QP2010SE GC MS instrument.

RESULTS AND DISCUSSION

DwCNT Functionalization. Pristine dwCNT samples contain some bundles of CNTs, as well as some diaphanous carbon, and are hydrophobic (Figure 1a). Acidic treatments are commonly used for the cleaning and functionalization of CNTs.[27−29] The two major purposes are (i) a purification stage with the removal of the diaphanous carbon and elimination of the residual catalytic Co:Mo nanoparticles and (ii) a functionalization stage with the generation of oxygen rich functions (hydroxyl, carbonyl, and carboxyl) at the surface of the CNTs. In the frame of this study, we have chosen two main acidic treatments for the purification and functionalization of the dwCNTs: the single HNO_3 oxidation stage or the double oxidation stage with a first HNO_3 treatment followed by a second oxidation with a mixture of HNO_3 and H_2SO_4. These treatments allow the covalent grafting of about 3.7 mmol of surface oxygen groups per gram of CNTs on the outer CNT walls.[27] These functions are required to increase the chemical interaction between the metalorganic copper precursors and carbon, therefore leading to the formation of numerous nucleation sites for copper at the substrate surface. After the first HNO_3 acidic stage (see the Experimental Section), up to 90% of the catalytic metal particles (measured by ICP AES) and some of the amorphous carbon are removed. The yield of the reaction is 80 wt %.[27] One can notice the presence of carboxylated carbonaceous fragments (CCFs) at the surface of CNTs and between CNT bundles after this treatment (Figure 1b). These CCFs are amorphous carbon layers originating from the oxidative attack of diaphanous carbon and CNT walls by nitrous acid.[30] Up to 96% of the initial metal traces and even more carbon are eliminated after the second acidic treatment with H_2SO_4. However, this stage is very aggressive for the CNTs since the final reaction yield falls down to only 20% of the initial mass.[27] This very low yield suggests that not only the disorganized carbon but also the sp^2 carbon network of the CNT walls is strongly attacked by the sulfuric acid mixture.

Indeed, functionalized CNTs exhibit higher structural integrity than pristine CNTs with the Raman I_D/I_G ratio decreasing from 0.20 to 0.08, respectively.[27] It is noteworthy that after the second acidic attack most of the dwCNTs are self assembled into thick bundles (several tens of nm large), and only very few single CNTs are evidenced (Figure 1c). In addition, the surface of CNT bundles is rather rough and surrounded by a matrix of disordered carbonaceous film (CCFs) embedding the CNTs as a result of the strong acidic attack of the dwCNTs and diaphanous carbon. These CCFs, usually regarded as an unwanted impurity for CNTs, may be removed by further washing with a solution of NaOH.[27,31] However, for the purpose of this study, we have chosen to keep the CCFs since these oxidized species may advantageously play the role of anchoring sites for metalorganic copper precursors.

CuNPs@dwCNTs Characterizations. Figure 2 presents the TEM analysis of the decorated Cu@CNTs according to

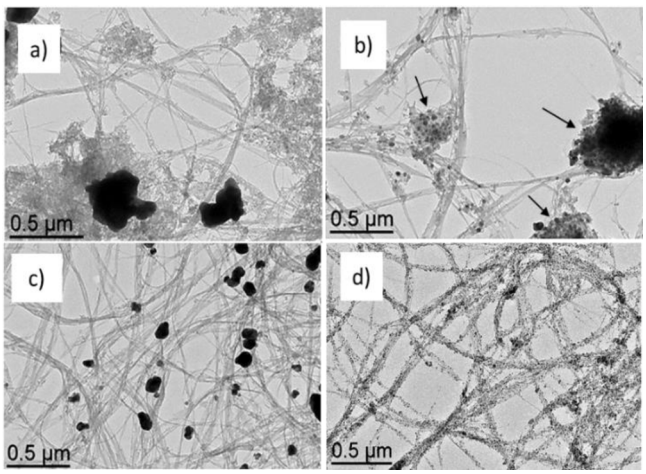

Figure 2. TEM images of Cu@CNTs using a) CuAmd on single oxidized CNTs, b) CuMes on single oxidized CNTs (Arrows indicate the presence of CCFs and Cu NPs.), c) CuAmd on double oxidized CNTs, and d) CuMes on double oxidized CNTs.

the different experimental conditions. The dwCNT decoration strongly depends on the CNT functionalization and the composition of copper precursors. In the case of CuAmd, only large and shapeless copper agglomerates (from 100 nm to several hundred of nm) erratically appear on the CNTs

whatever the functionalization (Figures 2a and 2c). A slight decrease of the agglomerates size (Cu NP mean size 94 ± 30 nm) and distribution over the CNTs is obtained for double oxidized CNTs (Figure 2c). This inhomogeneous decoration of the CNTs by the Cu correlates well with the macroscopic aspect of the Fisher Porter vessel after the reaction, since a shiny copper mirror also covers the glass walls (Figure S1a in the SI).

This reflects the higher affinity of CuAmd for the SiOH functions present on the glass vessel rather than for the oxidized carbonaceous functions present on the CNTs in suspension. Indeed, it has already been demonstrated that the copper amidinate precursor is particularly well suited for the formation of regular copper films on functionalized silicon substrates.[32] On the contrary, using CuMes, a better decoration of CNTs by Cu NPs is observed whatever the CNT functionalization. Importantly, there are no NPs found apart from the dwCNTs on the TEM grid. Moreover, it is worth noting that in the absence of any CNTs in anisole, Cu^0 NPs grow as a colloidal solution, and a bright copper film eventually covers the reactor walls.[19] This strongly suggests that an acid functionalization of dwCNTs provides good ligands for the chelation of copper species and grafting of Cu NPs. Single oxidization treatment allows the formation of Cu NPs with rather narrow size distribution (mean size 29 ± 10 nm) (Figure 2b). However, the distribution of Cu NPs is not homogeneous in the sample. The nucleation and growth of Cu NPs appear preferentially on the diaphanous carbon areas rather than directly on the walls of the dwCNTs. The optimized decoration condition is achieved with double oxidized CNTs, i.e., that bear a high amount of CCFs (Figure 2d). Small size Cu NPs with narrow size distribution (mean size 9.2 ± 3.0 nm) regularly decorate the CNT bundles (Figures 3a,b and S2 of the SI). This suggests that the CCFs possess a high density of functionalized sites used for copper chelation and growth. A high resolution TEM (HRTEM) analysis of the sample shows that a disorganized carbon layer (CCFs) regularly covers the dwCNTs (Figure 3c).

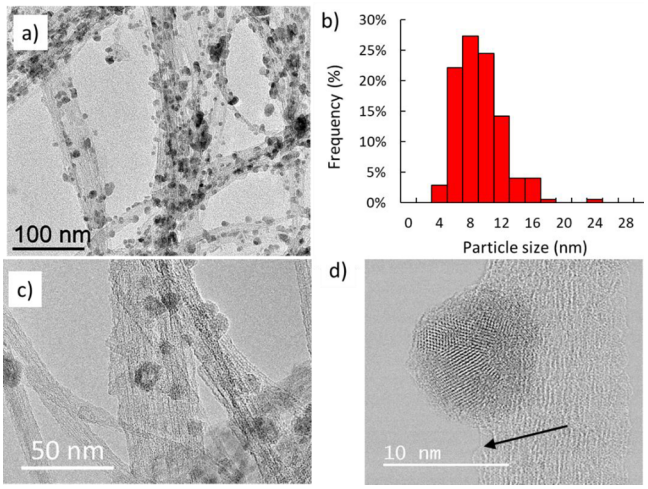

Figure 3. a) TEM image of double oxidized CNTs decorated by CuNPs obtained from CuMes, b) histogram of size distribution of Cu NPs, and HRTEM images of c) CuNPs on CNT bundles and d) CuNPs located between two CNT bundles (The arrow indicates the presence of CCFs on the CNTs.).

The growth of Cu NPs seems to occur preferentially on amorphous carbon coatings rather than directly on clean CNT walls (Figures 3d and S3 in the SI). This confirms that the CCFs generated by the second oxidation step of CNTs contain a high density of defects where CuMes can react and generate nucleation sites for further Cu growth. Due to the synthesis conditions under reducing atmosphere (dihydrogen pressure), the as prepared Cu NPs are produced under their metallic Cu^0 form.[19] However, the deposition of the samples on the microscopy grids under ambient air induces at least a partial transformation of Cu nanocrystals into copper oxides. Cu NPs appear to be polycrystalline (Figure 3d), and Fourier transform (FT) analyses of the measured polycrystals more often reveal cubic Cu_2O arrangements and some residual Cu^0 structures (Figure S4 in the SI). In HAADF STEM conditions, it is possible to obtain atomic resolution images with a chemical contrast linked to the atomic number of the elements (Z contrast image). This analysis mode revealed a very interesting feature on the Cu@dwCNTs. They consist not only of well defined Cu nanocrystals (Figure 4a) but also of a large amount

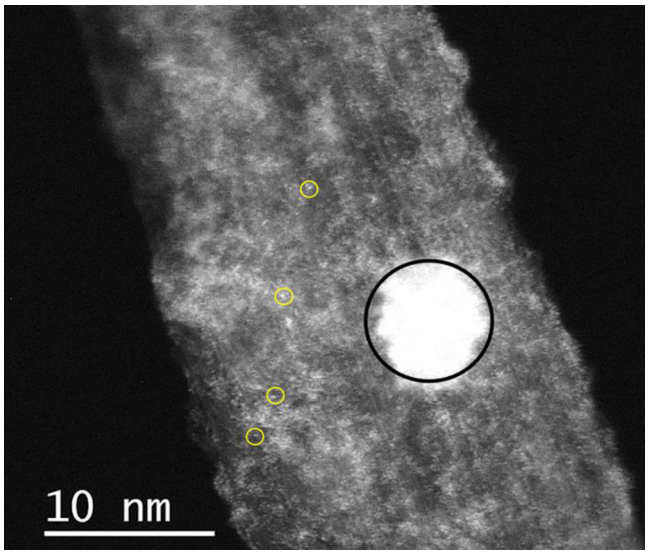

Figure 4. HRTEM STEM HAADF image of the CNT bundle showing a CuNP (black circle) and the multiple grafting of Cu all along the CNT bundle (Four Cu atoms/clusters are surrounded by yellow circles to guide the eye; each white spot on the image corresponds to a copper atom/cluster.).

of copper atoms or small clusters that spread all along the CNT bundle surface. We clearly evidenced this atomic copper dispersion not only near the Cu NPs but also on every CNT zone far from Cu NPs (Figures 4b and S5 in the SI).

STEM EDX analyses only reveal C, Cu, and O elements from the sample and the Ni signal coming from the TEM grid (Figure S6 in the SI). Elemental copper appears whenever the analysis focuses on a Cu NP or on a zone without any directly observable NPs (Figure S6b in the SI). This unambiguously confirms the presence of elementary copper all along the dwCNTs. The reactivity of surface metallic atoms has gone unnoticed in recent decades, but Qiao et al. have remarkably shed light on it with a new perspective with the concept of single atom catalysis (SAC) and its achievements.[33] As an example, Johnston's pioneering work highlighted the important role of monometallic gold on carbon materials for the industrial catalysis of vinyl chloride monomer.[34] In the case

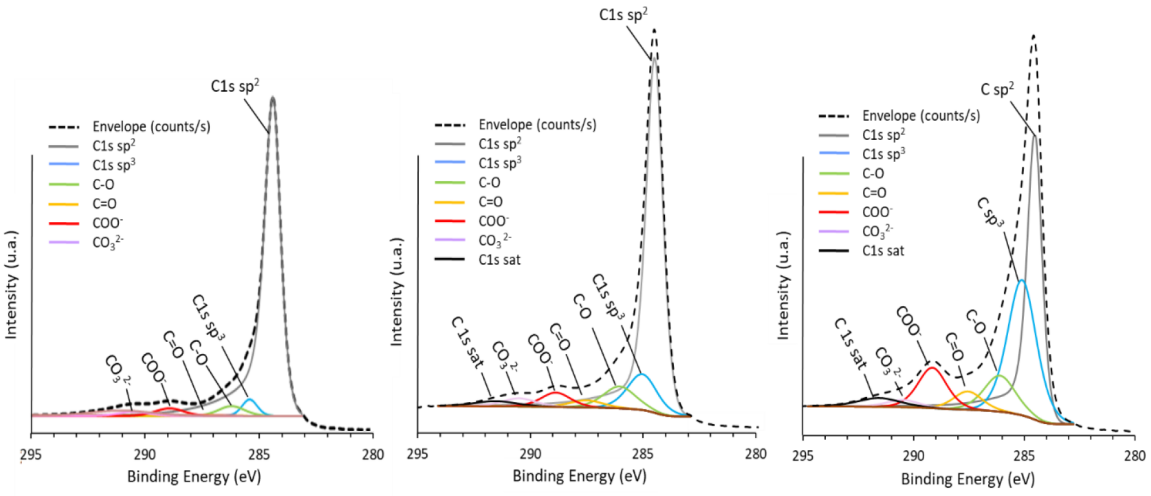

Figure 5. Deconvolution of XPS C 1s peaks of a) raw CNTs, b) single oxidized CNTs, and c) double oxidized CNTs.

Table 1. Atomic Contents (at. %) of Carbon Hybridization and Elements in dwCNTs Measured by XPS Fits of the C 1s Spectra and Survey

	C 1s sp^2	C 1s sp^3	C 1s C O	C 1s C O	C 1s C OO	C 1s CO_3	C 1s sat.	O 1s oxides	N 1s	S 2p	Mo 3d	Co $2p_{3/2}$	Cu $2p_{3/2}$
pristine dwCNTs	79.7	3.1	3.0	0.3	2.8	1.6	4.5	5			0.1	0.2	
single-oxidized dwCNTs	62.6	9.6	6.5	2.2	3.9	2.5	1.9	10.1	0.8				
double-oxidized dwCNTs	33.5	26.2	7.7	3.6	7.9	1.6	2.5	17.0		0.1			
Cu @ double-oxidized dwCMs	35.2	29.4	5.4	1.9	4.0	0.7	0.6	17.1	1.3				4.4

of heterogeneous catalytic reactions, the atomic dispersion of a metal on a surface is very appropriate since the reactivity of metallic clusters essentially depends on the availability of surface atoms. The atomic decoration of a substrate necessitates a very strong metal−support interaction in order to restrict the atoms' surface mobility and their eventual transformation into clusters or nanoparticles with time. Hence, the presence of chelating functions on a surface is a prerequisite to foster the adsorption of metal centers and also to limit their mobility under harsh catalytic reaction conditions. The double oxidation treatment of dwCNTs generates a high density of efficient anchoring sites on the CCFs covering the CNTs, which consequently promote the stabilization of copper at the atomic level.

XPS analyses were performed on pristine and functionalized CNTs in order to evidence the modification of the CNTs by acidic solutions. Figure S7 in the SI shows the XPS survey spectra with C 1s peaks and O 1s respectively located at binding energies (B.E.) of 285 and 530 eV. Very small peaks corresponding to residual Mo (B.E. = 230 eV) and Co (B.E. = 780 eV) from the starting catalyst material appear only in raw dwCNT analysis. These peaks disappear for the two acid treated CNTs (single and double oxidation) which confirms their efficiency for the purification of the CNTs down to the detection limit of the XPS system (100 ppm). Note that eventual residual metal particles (Co or Mo) not eliminated by H_2SO_4 treatment are encapsulated in carbon shells. They are thus very unlikely to play a role in further catalytic reactions. Figure 5 presents C 1s peak envelopes and their deconvolution. The analysis of C 1s peaks from CNTs reveals seven different contributions described by Chiang et al.[35] The structural state of carbon in the pristine dwCNTs shows a major peak corresponding to the graphitic sp^2 carbon (B.E. = 284.6 eV) corresponding to the CNT walls and a much lower one at 285.4 eV attributed to a disorganized sp^3 carbon. The C 1s deconvolution also reveals four other contributions corresponding to carbon in an oxygen rich environment like hydroxyl (C−O, B.E. = 286 eV), carbonyl (C═O, B.E. = 287.6 eV), carboxyl (C−OO, B.E. = 288.8 eV), and adsorbed carbonate (CO_3, B.E. = 290.6 eV, possible overlap with the binding energy range of the C 1s shakeup response) groups. These oxygen rich environments correspond to possible anchoring sites for copper precursors or metal atoms. The very last and very small contribution to the C 1s peak envelope is due to a small satellite peak of carbon due to $\pi-\pi$ transition in aromatic rings (B.E. = 291.6 eV).

Table 1 presents the atomic percentages of the main elements and the carbon involved in chemical functions on the dwCNTs. The C 1s sp^2 peak is representative of the carbon forming the regular hexagonal network of the CNTs. The atomic proportion of C 1s sp^2, relative to the total sp^2 and sp^3 amounts, decreases from around 96% in pristine material to 86% after a single oxidation stage and drops abruptly to 56% for double oxidized CNTs. Simultaneously, the amount of disordered carbon measured by the C 1s sp^3 percentage is multiplied by 12 between the pristine sample to the double oxidized one. This result correlates the HRTEM observations of this sample revealing an amorphous carbon layer embedding the dwCNT bundles and especially after double oxidation. In addition, this sp^3 carbon increase is correlated with a high level of oxygen groups in the sample. A net increase of the oxygenated functional carbon is measured for acid treated dwCNTs. Double oxidized CNTs exhibit up to 20.6 at. % of oxygen environed carbon (sum of C−O, C═O, COO, and CO_3), whereas it is only 15.1 at. % for single oxidized CNTs and 7.7 at. % for pristine CNTs. Finally, the chelating functions

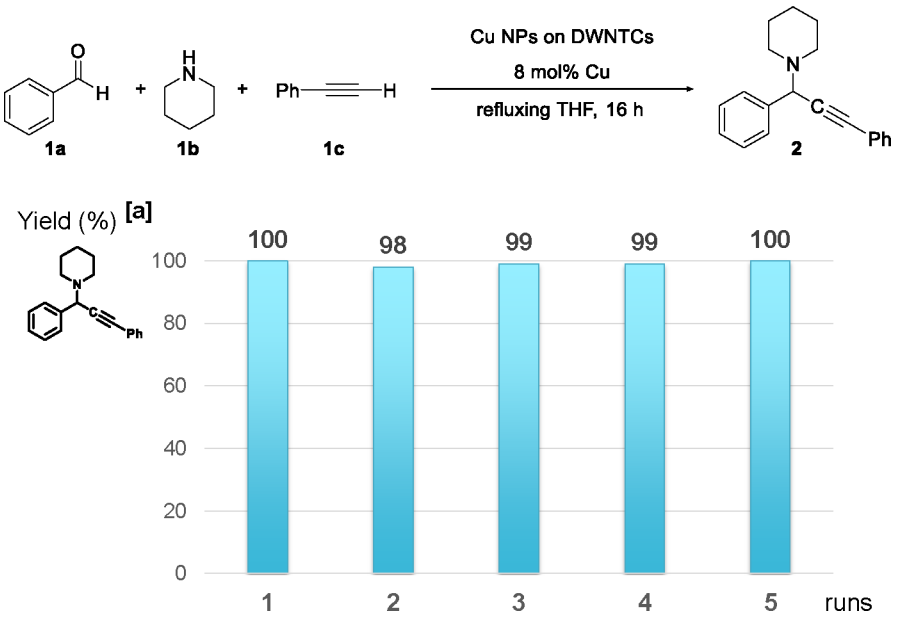

Figure 6. A^3 coupling involving benzaldehyde, piperidine, and phenylacetylene (1:1:1 ratio; 1.2 mmol scale): catalytic performances and recycling abilities of the Cu NPs dispersed and stabilized on the dwCNTs. [a]Yields determined according to ^{1}H NMR spectra. For run 5: the product has been isolated by a simple filtration of the crude through a pad of Celite 545 (isolated yield of 99%, see the SI for the details on the procedure for the catalytic reactions and recycling experiments).

for Cu atoms on dwCNT bundles are carried by defective sp^3 carbon and especially by CO^- and COO^- species that represent the major part of the functionalized carbon (15.6 at. %) in double oxidized CNTs. After Cu decoration, the XPS analysis reveals the presence of 4.4 at. % of copper and up to 77.2 at. % of carbon (Table 1). This copper amount related to the total carbon corresponds to a level of 5.7% that is very close to the copper amount initially introduced in the reaction (molar ratio Cu/C = 6.5 at. %). This shows that about 95% of copper involved in the reaction is grafted on the dwCNTs. There is no loss of copper, either by condensation on the reactor walls or as free NPs formed in solution. The overall amount of the oxygen rich carbon species has decreased after Cu decoration (from 20.6 at. % before Cu deposition to 12 at. % after deposition) which suggests their partial consumption due to the reducing conditions under dihydrogen pressure.

Evaluation of the Catalytic Activity of the Nanocomposite in One Benchmark A^3-Coupling. The coex istence of Cu nanocrystals, small clusters, and copper single atoms on the dwCNTs prompted us to evaluate the behavior of this nanocomposite in one benchmark reaction for which copper based catalysts are of choice: the A^3 coupling. This one pot three component reaction gives rise to propargyl amines, key compounds in organic chemistry and versatile precursors of nitrogen containing heterocycles, natural prod ucts, and biologically active molecules.[36−38] Compared to the classical route to propargylamines consisting of the addition of a metal acetylide to an imine, the A^3 coupling is a straightforward, atom economic, and more sustainable route. It can be promoted by molecular catalysts based on several transition metals including copper, gold, silver, nickel, zinc, or palladium. However, the corresponding salts or complexes are hardly separated from the expected product, and metal NPs acting as recoverable heterogeneous catalysts constitute a competitive alternative. Therefore, copper, gold, or silver NPs have been efficiently applied in A^3 couplings, and cheaper copper NPs (Cu, Cu_2O, CuO, or possibly hybrid in terms of Cu oxidation degrees) are highly attractive.[39] One main and general drawback with metal NPs is that agglomeration and coagulation generally observed lead to a significant decrease of the catalytic performances. Supporting the metal NPs on metal oxides, silica, zeolite, carbon, or polymeric matrices constitutes one way to solve this problem, and this approach is attracting growing interest.[39−44] Along these lines, the Cu NPs dispersed and stabilized on the dwCNTs appear as relevant hybrid nanomaterials for catalyzing a model A^3 coupling involving benzaldehyde **1a**, piperidine **1b**, and phenylacetylene **1c** (Figure 6). An equimolar mixture of these three substrates is allowed to react in the presence of the hybrid materials in refluxing THF under stirring. After 16 h, the nanocomposite is isolated from the reaction solution by centrifugation and rinsing with THF twice. The supernatants are gathered, and the THF is removed under vacuum to quantitatively yield the expected propargylamine (Figure 6, Cycle 1) according to the ^{1}H NMR spectrum of the crude product. Although the time required to go to completion (16 h) is quite long, the temperature conditions (65 °C) are among the mildest reported, and many related systems involving Cu NPs dispersed on supports often require a temperature of 90−100 °C for complete conversion of reactants (see Table S1 in the SI for recent reports). It is worthy to note that the double oxidized dwCNTs (without Cu deposition) are unable to promote the reaction which therefore precludes the role of residual Co or Mo particles in the catalytic performance. Next, the recycling abilities of the recovered Cu@dwCNTs have been successfully evaluated since the catalytic material could be used for five consecutive runs with no loss of activity (Figure 6, reaction time = 16 h, time required to consume all reagents **1a**, **1b**, and **1c**, determined for run 1).

Such recycling performances are on the average of those obtained in related CuNPs dispersed on various supports including N doped CNTs (see Table S1).[23] Interestingly, even for the fifth cycle, the catalytic reaction occurs quantitatively and selectively from the equimolar mixture of reactants **1a**, **1b**,

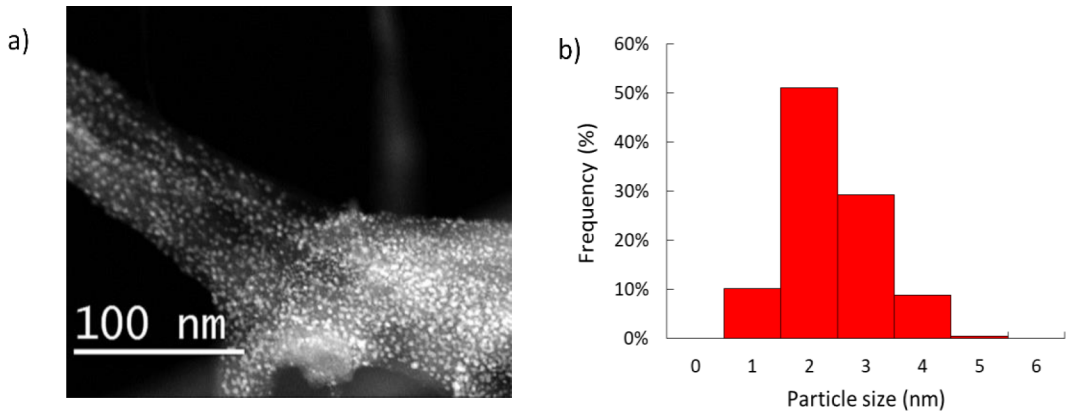

Figure 7. a) HAADF STEM image showing the homogeneous Cu NP dispersion on the CNT bundles after five catalytic cycles and b) histogram of NP size distribution.

and **1c**, and no purification by column chromatography is needed, propargylamine **2** being isolated pure by a simple filtration through a pad of Celite 545 (see the SI for details, Figures S8 and S9 in the SI). This constitutes a strong advantage of the method. Investigations are next carried out on the morphology and composition of the catalytic system after catalysis.

Analyses of the Nanocomposite after Catalytic Tests. The Cu@dwCNTs nanocomposites employed for five consecutive catalytic reactions have been analyzed by HRTEM (Figure 7). Surprisingly, the Cu nanocrystal distribution on dwCNTs has evolved toward much smaller particles size (mean size 2.4 ± 0.7 nm). The general aspect of the dwCNTs has not changed; they are still assembled into bundles (Figure S10 in the SI). The Cu nanocrystals homogeneously cover the CNTs (Figure S11 in the SI). The catalytic reaction conditions (65 °C in THF, in the presence of aldehyde **1a**, amine **1b**, and alkyne **1c** compounds) seem to be harsh enough to favor the redissolution of the large Cu nanoparticles into smaller ones. Generally, the thermodynamic evolution of NPs with temperature and time leads to a coarsening effect to minimize their surface energy. This mechanism is due to the Ostwald ripening where small particles can redissolve in solution and participate in the growth of larger particles.[45] Conversely, during the synthesis of propargylamines, the largest copper NPs undergo a redis solution mechanism to finally yield a lower NP mean size grafted on the CNTs. The recently described reverse Ostwald ripening[46] (or reverse coarsening) process, where the growth of smaller nanocrystals is favored at the expense of larger ones, may drive the observed evolution. This effect is observed in the particular case where the ligands attached to the surface atoms of the metal cluster can produce a negative surface energy. According to Bootharaju et al.,[47] the classical Ostwald ripening process is driven by the tendency of the cluster to decrease the total surface energy toward a minimum. However, in the case where the ligand surface binding energy is high enough, it produces a negative surface energy driving to the lowering of the cluster size. In our case where two competitive ligands are involved (strong carboxyl ligands at the CNT surface and labile amine ligands in solution), we assume that the observed mean size reduction of copper particles after catalysis is due to the reverse Ostwald ripening due to strong carboxyl ligands present on acidified dwCNT. The small Cu NPs remaining on dwCNTs may represent the nanocrystal size corresponding to the balance where the binding energy from the carboxyl ligands at the CNT surface becomes higher than the one of the amine ligands in solution.

Remarkably, the persistence of a high surface density of atomic copper on the bundles evidenced by HAADF STEM on a sample after five successive catalytic cycles supports this hypothesis (Figure 8).

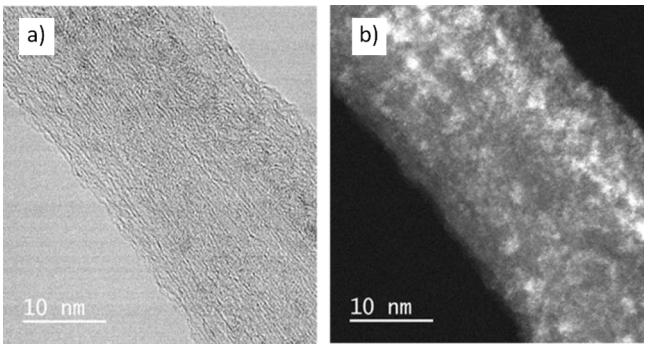

Figure 8. HRTEM images evidencing Cu atoms still grafted on the CNT bundles after five consecutive catalytic cycles: a) bright field and b) HAADF STEM image.

The FT analyses of the sample after five catalytic samples are difficult to interpret due to the smaller size of the diffracting entities. However, we evidenced the presence of CuO and Cu_2O compounds (Figure S12a,b in the SI). XPS analysis also confirmed the oxidation level of copper (Figure S13 in the SI). The Cu 2p characteristics indicate a mixture of Cu_2O (B.E. = at 953 and 933 eV) and CuO or $Cu(OH)_2$ compounds (B.E. = shoulders at 954 and 934 eV). The relatively strong satellite peaks located at B.E. = 963 and 941 eV are also in favor of the presence of Cu^{2+} species on the sample. This analysis confirms the good stability of copper decoration on dwCNT bundles after five successive catalytic cycles. After catalysis, the XPS atomic quantification reveals a notable decrease of the Cu present in the sample with an overall of 2.3 at. %, which corresponds to 2.9 at. % relative to the carbon amount (Table 2). This evolution correlates well with the HRTEM observation of a decrease in the Cu NP mean size due to redissolution effects. The mass transport mechanism inevitably leads to the loss of part of the copper in the solution during the catalytic cycles. However, the catalytic yield remains quantitative even for the fifth cycle. It means that enough

Table 2. Atomic Contents (%) of Carbon Hybridization and Elements in dwCNTs after 5 Catalysis Cycles Measured by XPS Fits of the C 1s Spectra and Survey

C 1s sp^2	C 1s sp^3	C 1s C O	C 1s C O	C 1s C OO	C 1s CO_3	C 1s sat.	O 1s oxides	N 1s	Cu $2p_{3/2}$
31.5	39.5	4.6	2.2	1.1	0	1	15.6	2.3	2.3

catalytic species remain available on dwCNTs to promote a complete catalytic run. The 100% yield achieved after five cycles suggests that 2.3 at. % Cu, under NPs and single atom form, is already enough to offer very efficient catalytic properties. The dwCNT external walls present a disorganized sp^3 carbon layer bearing oxygen species formed during the double oxidation step, on which Cu atoms as well as Cu NPs are bonded. These atoms and NPs are mainly present as oxidized Cu species, and the latter possibly contributed to the catalytic synthesis of propargylamines. Such a phenomenon would be consistent with the well known ability of copper precursors with various oxidation degrees (0, 1, or 2) to promote A^3 coupling.[36,39−44]

The importance of the size of the NPs as well as of the contribution of atomic Cu versus Cu NPs on the catalytic reaction yield are still to be elucidated. A further work will aim to shed some light on the nature of the real catalytic active species. Moreover, the fact that the quantitative activity is maintained with a significantly lower amount of copper on dwCNTs (Cu 2.3% at.) after catalysis indicates that it could be possible to decrease the initial copper content. The future studies on Cu@dwCNTs nanocomposites will target their selective decoration with atomically dispersed Cu, in order to assess a purely atoms controlled type catalytic reaction.

CONCLUSIONS

In summary, tailoring dwCNT functionalization and Cu NP synthesis conditions, we have synthesized Cu@CNTs nano composites that demonstrated high efficiency and durability for propargylamine catalysis. The functionalization of dwCNTs leads to the formation of a matrix of amorphous carbon (CCFs) all around the dwCNTs and hence promoting their self assembly into bundles. This disorganized carbon lining exhibits a dense source of hydroxyl and carboxyl functions, allowing an outstanding chelating capability for copper atoms. Accordingly, the decomposition of mesityl copper under a moderate H_2 pressure leads to the homogeneous decoration of CNT bundles with Cu NPs (9.2 ± 3.0 nm). Noteworthy, in addition to the regular NP distribution, we evidenced the regular spreading of copper atoms on the packed CNT surface. When the copper precursor starts to decompose, the scavenging functions on the amorphous carbon layer are occupied by copper atoms, and the atomic adsorption continues up to the point where Cu NPs regularly grow over the dwCNT bundles. This nanocomposite material has been successfully employed in the A^3 type coupling catalytic reaction for the synthesis of a propargylamine derivative. Up to 5 catalytic cycles have been successively run with quantitative yield, and the catalyst is easily recovered by centrifugation after each run. We also demonstrated the remarkable reorganization of copper NPs at the surface of dwCNTs after catalytic cycles where the Cu NP mean size decreases to 2.4 ± 0.7 nm. A possible reverse Ostwald process may drive this structural evolution where the largest Cu NPs are redissolved during the catalytic reaction, while both smaller NPs and atomic Cu decoration remain. This effect underlines the very efficient chemical interaction between Cu and carboxyl functions present on the carbonaceous support.

ASSOCIATED CONTENT

Supporting Information

The Supporting Information is available free of charge at https://pubs.acs.org/doi/10.1021/acs.langmuir.2c00771.

Procedure for catalytic reactions and recycling experiments, image of reactors after Cu deposition on dwCNTs, STEM HAADF of Cu dispersion on dwCNTs, HRTEM image of Cu NPs on CCFs, HRTEM image of NPs (center), and FT analysis of Cu nanocrystals, HRTEM image of dwCNT bundle, STEM EDX analyses of Cu NPs on dwCNT bundles, XPS survey spectra of CNTs, ^{1}H NMR spectrum of isolated propargylamine, GC MS chromatogram and mass spectrum of isolated propargylamine, TEM image of Cu@dwCNT bundles after five catalytic runs, HRTEM image of Cu@dwCNT bundles after five catalytic runs, STEM HAADF and HRTEM images of a Cu NP, XPS Cu 2p analysis of Cu@dwCNTs after five catalytic cycles, and table of conditions for recently reported A^3 coupling reactions catalyzed by nano composites (PDF)

AUTHOR INFORMATION

Corresponding Authors

Pierre Fau − *LCC CNRS (Laboratoire de Chimie de Coordination), F 31077 Toulouse, France; Université de Toulouse, UT 3 Paul Sabatier, F 31062 Toulouse Cedex 9, France;* orcid.org/0000 0003 0014 2511; Email: pierre.fau@insa toulouse.fr

Armelle Ouali − *Institut Charles Gerhardt, UMR5253 Ecole Nationale Supérieure de Chimie de Montpellier, 34296 Montpellier, France;* orcid.org/0000 0001 7436 776X; Email: armelle.ouali@enscm.fr

David Mesguich − *CIRIMAT, Université de Toulouse, CNRS INPT UPS, Université de Toulouse 3 Paul Sabatier, F 31062 Toulouse, France;* orcid.org/0000 0002 4479 1292; Email: david.mesguich@univ tlse3.fr

Authors

Lilian Moumaneix − *CIRIMAT, Université de Toulouse, CNRS INPT UPS, Université de Toulouse 3 Paul Sabatier, F 31062 Toulouse, France; LCC CNRS (Laboratoire de Chimie de Coordination), F 31077 Toulouse, France*

Victor Henri − *CIRIMAT, Université de Toulouse, CNRS INPT UPS, Université de Toulouse 3 Paul Sabatier, F 31062 Toulouse, France; LCC CNRS (Laboratoire de Chimie de Coordination), F 31077 Toulouse, France*

Morgan Legnani − *CIRIMAT, Université de Toulouse, CNRS INPT UPS, Université de Toulouse 3 Paul Sabatier, F 31062 Toulouse, France; LCC CNRS (Laboratoire de Chimie de Coordination), F 31077 Toulouse, France*

Vincent Collière − *LCC CNRS (Laboratoire de Chimie de Coordination), F 31077 Toulouse, France; Université de*

Toulouse, UT 3 Paul Sabatier, F 31062 Toulouse Cedex 9, France

Jérôme Esvan − *CIRIMAT, Université de Toulouse, CNRS INPT UPS, 31030 Toulouse, France*

Complete contact information is available at: https://pubs.acs.org/10.1021/acs.langmuir.2c00771

Author Contributions

D.M. conceived the study, prepared the dwCNTs, interpreted the results, and wrote the manuscript. L.M., V.H., and M.L. prepared the dwCNTs and ran the hydrogenolysis experiments with Cu NPs. V.C. performed the TEM and HRTEM characterizations and analyses. J.E. performed the XPS characterizations and wrote the manuscript. A.O. conceived the study, ran the catalytic experiments, interpreted the results, and wrote the manuscript. P.F. conceived the study, designed and performed dwCNT decoration experiments, interpreted the results, wrote, and edited the manuscript.

Notes

The authors declare no competing financial interest.

■ ACKNOWLEDGMENTS

We thank the French Centre National de la Recherche Scientifique (CNRS), Université Fédérale de Toulouse (UFT) UT3 Paul Sabatier, and Institut Charles Gerhardt (ICGM). The Microcharacterization Centre Raimond Castaing is also acknowledged for technical support. We thank E. Flahaut for proofreading the paper and providing valuable expertise on CNT functionalization.

■ REFERENCES

(1) Erdelyi, B.; Orinak, A.; Orinakova, R.; Lorincik, J.; Jerigova, M.; Velic, D.; Micusik, M.; Omastova, M.; Smith, R. M.; Girman, V. Catalytic activity of mono and bimetallic Zn/Cu/MWCNTs catalysts for the thermocatalyzed conversion of methane to hydrogen. *Appl. Surf. Sci.* **2017**, *396*, 574−581.

(2) Wu, J.; Lu, H.; Zhang, X.; Raziq, F.; Qu, Y.; Jing, L. Enhanced charge separation of rutile TiO2 nanorods by trapping holes and transferring electrons for efficient cocatalyst free photocatalytic conversion of CO2 to fuels. *Chem. Commun. (Cambridge, U. K.)* **2016**, *52* (28), 5027−5029.

(3) Akbayrak, S.; Ozkar, S. Ruthenium(0) Nanoparticles Supported on Multiwalled Carbon Nanotube As Highly Active Catalyst for Hydrogen Generation from Ammonia Borane. *ACS Appl. Mater. Interfaces* **2012**, *4* (11), 6302−6310.

(4) Lin, K. S.; Mai, Y. J.; Li, S. R.; Shu, C. W.; Wang, C. H. Characterization and hydrogen storage of surface modified multi walled carbon nanotubes for fuel cell application. *J. Nanomater.* **2012**, *2012*, 939683.

(5) Shezad, N.; Maafa, I. M.; Johari, K.; Hafeez, A.; Akhter, P.; Shabir, M.; Raza, A.; Anjum, H.; Hussain, M.; Tahir, M. Carbon nanotubes incorporated Z scheme assembly of AgBr/TiO2 for photocatalytic hydrogen production under visible light irradiations. *Nanomaterials* **2019**, *9* (12), 1767.

(6) Manzetti, S.; Gabriel, J. C. P. Methods for dispersing carbon nanotubes for nanotechnology applications: liquid nanocrystals, suspensions, polyelectrolytes, colloids and organization control. *International Nano Letters* **2019**, *9* (1), 31−49.

(7) Kumar, S.; Pavelyev, V.; Mishra, P.; Tripathi, N. A review on chemiresistive gas sensors based on carbon nanotubes: Device and technology transformation. *Sensors and Actuators, A: Physical* **2018**, *283*, 174−186.

(8) Palza, H.; Saldias, N.; Arriagada, P.; Palma, P.; Sanchez, J. Antibacterial Carbon Nanotubes by Impregnation with Copper Nanostructures. *Jom* **2017**, *69* (8), 1319−1324.

(9) Nichols, F.; Lu, J. E.; Mercado, R.; Rojas Andrade, M. D.; Ning, S.; Azhar, Z.; Sandhu, J.; Cazares, R.; Saltikov, C.; Chen, S. Antibacterial Activity of Nitrogen Doped Carbon Dots Enhanced by Atomic Dispersion of Copper. *Langmuir* **2020**, *36* (39), 11629−11636.

(10) Georgakilas, V.; Gournis, D.; Tzitzios, V.; Pasquato, L.; Guldi, D. M.; Prato, M. Decorating carbon nanotubes with metal or semiconductor nanoparticles. *J. Mater. Chem.* **2007**, *17* (26), 2679−2694.

(11) Belesi, M.; Panagiotopoulos, I.; Pal, S.; Hariharan, S.; Tsitrouli, D.; Papavassiliou, G.; Niarchos, D.; Boukos, N.; Fardis, M.; Tzitzios, V. Decoration of carbon nanotubes with CoO and Co nanoparticles. *J. Nanomater.* **2011**, *2011*, 320516.

(12) Kardimi, K.; Tsoufis, T.; Tomou, A.; Kooi, B. J.; Prodromidis, M. I.; Gournis, D. Synthesis and characterization of carbon nanotubes decorated with Pt and PtRu nanoparticles and assessment of their electrocatalytic performance. *Int. J. Hydrogen Energy* **2012**, *37* (2), 1243−1253.

(13) Xu, J. B.; Zhao, T. S. Synthesis of well dispersed Pt/carbon nanotubes catalyst using dimethylformamide as a cross link. *J. Power Sources* **2010**, *195* (4), 1071−1075.

(14) Li, J.; Zhou, Y.; Xiao, X.; Wang, W.; Wang, N.; Qian, W.; Chu, W. Regulation of Ni CNT Interaction on Mn Promoted Nickel Nanocatalysts Supported on Oxygenated CNTs for CO2 Selective Hydrogenation. *ACS Appl. Mater. Interfaces* **2018**, *10* (48), 41224−41236.

(15) Kharisov, B. I.; Kharissova, O. V.; Ortiz Mendez, U.; De La Fuente, I. G. Decoration of Carbon Nanotubes With Metal Nanoparticles: Recent Trends. *Synthesis and Reactivity in Inorganic, Metal Organic, and Nano Metal Chemistry* **2016**, *46* (1), 55−76.

(16) Hafez, I. H.; Berber, M. R.; Fujigaya, T.; Nakashima, N. High Electronic Conductivity and Air Stability of Ultrasmall Copper Metal Nanoparticles Supported on Pyridine Based Polybenzimidazole Carbon Nanotube Composite. *ChemCatChem.* **2017**, *9* (22), 4282−4286.

(17) Sheng, L.; Huang, S.; Sui, M.; Zhang, L.; She, L.; Chen, Y. Deposition of copper nanoparticles on multiwalled carbon nanotubes modified with poly (acrylic acid) and their antimicrobial application in water treatment. *Frontiers of Environmental Science & Engineering* **2015**, *9* (4), 625−633.

(18) Tahir, M.; Tahir, B.; Nawawi, M. G. M.; Hussain, M.; Muhammad, A. Cu NPs embedded 1D/2D CNTs/pCN hetero junction composite towards enhanced and continuous photocatalytic CO2 reduction to fuels. *Appl. Surf. Sci.* **2019**, *485*, 450−461.

(19) Barriere, C.; Alcaraz, G.; Margeat, O.; Fau, P.; Quoirin, J. B.; Anceau, C.; Chaudret, B. Copper nanoparticles and organometallic chemical liquid deposition (OMCLD) for substrate metallization. *J. Mater. Chem.* **2008**, *18* (26), 3084−3086.

(20) Silva, M. M.; Ribeiro, D.; Cunha, E.; Proenca, M. F.; Young, R. J.; Paiva, M. C. A simple method for anchoring silver and copper nanoparticles on single wall carbon nanotubes. *Nanomaterials* **2019**, *9* (10), 1416.

(21) Lomeli Rosales, D. A.; Delgado, J. A.; Diaz de los Bernardos, M.; Perez Rodriguez, S.; Gual, A.; Claver, C.; Godard, C. A General One Pot Methodology for the Preparation of Mono and Bimetallic Nanoparticles Supported on Carbon Nanotubes: Application in the Semi hydrogenation of Alkynes and Acetylene. *Chem.—Eur. J.* **2019**, *25* (35), 8321−8331.

(22) Seo, Y.; Hwang, J.; Lee, E.; Kim, Y. J.; Lee, K.; Park, C.; Choi, Y.; Jeon, H.; Choi, J. Engineering copper nanoparticles synthesized on the surface of carbon nanotubes for anti microbial and anti biofilm applications. *Nanoscale* **2018**, *10* (33), 15529−15544.

(23) Ramu, V. G.; Bordoloi, A.; Nagaiah, T. C.; Schuhmann, W.; Muhler, M.; Cabrele, C. Copper nanoparticles stabilized on nitrogen doped carbon nanotubes as efficient and recyclable catalysts for alkyne/aldehyde/cyclic amine A3 type coupling reactions. *Applied Catalysis, A: General* **2012**, *431*−*432*, 88−94.

(24) Rivera Carcamo, C.; Serp, P. Single Atom Catalysts on Carbon Based Materials. *ChemCatChem.* **2018**, *10* (22), 5058−5091.

(25) Li, Z.; Barry, S. T.; Gordon, R. G. Synthesis and Character ization of Copper(I) Amidinates as Precursors for Atomic Layer Deposition (ALD) of Copper Metal. *Inorg. Chem.* **2005**, *44* (6), 1728−1735.
(26) Flahaut, E.; Bacsa, R.; Peigney, A.; Laurent, C. Gram scale CCVD synthesis of double walled carbon nanotubes. *Chem. Commun. (Cambridge, U. K.)* **2003**, No. 12, 1442−1443.
(27) Bortolamiol, T.; Lukanov, P.; Galibert, A. M.; Soula, B.; Lonchambon, P.; Datas, L.; Flahaut, E. Double walled carbon nanotubes: Quantitative purification assessment, balance between purification and degradation and solution filling as an evidence of opening. *Carbon* **2014**, *78*, 79−90.
(28) Maciejewska, B. M.; Jasiurkowska Delaporte, M.; Vasylenko, A. I.; Koziol, K. K.; Jurga, S. Experimental and theoretical studies on the mechanism for chemical oxidation of multiwalled carbon nanotubes. *RSC Adv.* **2014**, *4* (55), 28826−28831.
(29) Melchionna, M.; Prato, M. Functionalizing carbon nanotubes: an indispensable step towards applications. *ECS Journal of Solid State Science and Technology* **2013**, *2* (10), M3040−M3045.
(30) Salzmann, C. G.; Llewellyn, S. A.; Tobias, G.; Ward, M. A. H.; Huh, Y.; Green, M. L. H. The role of carboxylated carbonaceous fragments in the functionalization and spectroscopy of a single walled carbon nanotube material. *Adv. Mater. (Weinheim, Ger.)* **2007**, *19* (6), 883−887.
(31) Mortazavi, S. Z.; Novinrooz, A. J.; Reyhani, A.; Mirershadi, S. Effects of acid treatment duration and sulfuric acid molarity on purification of multi walled carbon nanotubes. *Central European Journal of Physics* **2010**, *8* (6), 940−946.
(32) Cure, J.; Piettre, K.; Sournia Saquet, A.; Coppel, Y.; Esvan, J.; Chaudret, B.; Fau, P. A Novel Method for the Metalization of 3D Silicon Induced by Metastable Copper Nanoparticles. *ACS Appl. Mater. Interfaces* **2018**, *10* (38), 32838−32848.
(33) Qiao, B.; Wang, A.; Yang, X.; Allard, L. F.; Jiang, Z.; Cui, Y.; Liu, J.; Li, J.; Zhang, T. Single atom catalysis of CO oxidation using Pt1/FeOx. *Nat. Chem.* **2011**, *3* (8), 634−641.
(34) Johnston, P.; Carthey, N.; Hutchings, G. J. Discovery, Development, and Commercialization of Gold Catalysts for Acetylene Hydrochlorination. *J. Am. Chem. Soc.* **2015**, *137* (46), 14548−14557.
(35) Chiang, Y. C.; Lin, W. H.; Chang, Y. C. The influence of treatment duration on multi walled carbon nanotubes functionalized by H2SO4/HNO3 oxidation. *Appl. Surf. Sci.* **2011**, *257* (6), 2401−2410.
(36) Jesin, I.; Nandi, G. C. Recent Advances in the A3 Coupling Reactions and their Applications. *Eur. J. Org. Chem.* **2019**, *2019* (16), 2704−2720.
(37) Peshkov, V. A.; Pereshivko, O. P.; Van der Eycken, E. V. A walk around the A3 coupling. *Chem. Soc. Rev.* **2012**, *41* (10), 3790−3807.
(38) Yogev Falach, M.; Amit, T.; Bar Am, O.; Youdim, M. B. H. The importance of propargylamine moiety in the anti Parkinson drug rasagiline and its derivatives for MAPK dependent amyloid precursor protein processing. *FASEB J.* **2003**, *17* (15), 2325−2327.
(39) Saha, T. K.; Das, R. Progress in Synthesis of Propargylamine and Its Derivatives by Nanoparticle Catalysis via A3 coupling: A Decade Update. *ChemistrySelect* **2018**, *3* (1), 147−169.
(40) Hekmati, M. Application of Biosynthesized CuO Nanoparticles Using Rosa canina Fruit Extract as a Recyclable and Heterogeneous Nanocatalyst for Alkyne/Aldehyde/Amine A3 Coupling Reactions. *Catal. Lett.* **2019**, *149* (8), 2325−2331.
(41) Muthukumar, P.; Kumar, P. S.; Anthony, S. P. Fabricating Cu, Cu2O and hybrid Cu Cu2O nanoparticles in carbon matrix and exploring catalytic activity of oxygen and hydrogen evolution and green A3 coupling reaction. *Materials Research Express* **2019**, *6* (2), 025518.
(42) Nasrollahzadeh, M.; Sajjadi, M.; Ghorbannezhad, F.; Sajadi, S. M. A Review on Recent Advances in the Application of Nanocatalysts in A3 Coupling Reactions. *Chem. Rec.* **2018**, *18* (10), 1409−1473.
(43) Patel, S. B.; Vasava, D. V. Azo functionalized polystyrene supported Copper nanoparticles: An economical and highly efficient catalyst for A3 and KA2 coupling reaction under microwave irradiation. *Nano Structures & Nano Objects* **2020**, *21*, 100416.
(44) Shaabani, A.; Shadi, M.; Mohammadian, R.; Javanbakht, S.; Nazeri, M. T.; Bahri, F. Multi component reaction functionalized chitosan complexed with copper nanoparticles: An efficient catalyst toward A3 coupling and click reactions in water. *Appl. Organomet. Chem.* **2019**, *33* (9), e5074.
(45) Gommes, C. J. Ostwald ripening of confined nanoparticles: chemomechanical coupling in nanopores. *Nanoscale* **2019**, *11* (15), 7386−7393.
(46) Sakar, M.; Balakumar, S. Reverse Ostwald ripening process induced dispersion of Cu2O nanoparticles in silver matrix and their interfacial mechanism mediated sunlight driven photocatalytic properties. *Journal of Photochemistry and Photobiology, A: Chemistry* **2018**, *356*, 150−158.
(47) Bootharaju, M. S.; Burlakov, V. M.; Besong, T. M. D.; Joshi, C. P.; AbdulHalim, L. G.; Black, D. M.; Whetten, R. L.; Goriely, A.; Bakr, O. M. Reversible Size Control of Silver Nanoclusters via Ligand Exchange. *Chem. Mater.* **2015**, *27* (12), 4289−4297.